Cyclotron resonance phenomena in a non-neutral multispecies ion plasma

E. Sarid,[a] F. Anderegg, and C. F. Driscoll
Institute for Pure and Applied Physical Sciences and Department of Physics, University of California at San Diego, La Jolla, California 92093

(Received 14 December 1994; accepted 1 May 1995)

Cyclotron modes of a non-neutral Mg ion plasma were studied in a long cylindrical Penning–Malmberg trap. Several modes with angular dependence $\exp(il\theta)$, $l \geqslant 1$, are observed near the cyclotron frequencies of the various Mg ions. The $l=1$ modes for the majority species are downshifted from the cyclotron frequencies, with downshifts as large as four times the diocotron frequency. These large shifts are quantitatively explained by a multispecies cold-plasma theory, including the dependence on the plasma size and composition. These dependencies allow the plasma size and composition to be obtained from the measured mode frequencies. In contrast, the $l=1$ downshifts for minority species are generally close to twice the diocotron frequency, and remain unexplained. Cyclotron heating of the plasma ions was also observed with a surprising effect of improving the plasma confinement. © *1995 American Institute of Physics.*

I. INTRODUCTION

In this paper we describe measurements and theory of the cyclotron modes of a non-neutral Mg ion plasma in a cylindrical Penning–Malmberg trap. In contrast to the extensive work done on low-frequency phenomena in non-neutral plasmas,[1] cyclotron modes were first observed by Gould and Lapointe[2] only recently in a pure electron plasma. The cyclotron modes are modified by the macroscopic equilibrium electric field and rotation of the plasma, giving shifts in the mode frequencies away from the single-particle cyclotron frequencies. The main difference between the ion plasma and electron plasma cyclotron modes[2] results from the multiple ion species, including two ionization states and three isotopes of Mg. While only one species supports a mode near a particular cyclotron resonance, the space charge associated with the other species contributes to frequency shifts of the resulting mode.

Ion cyclotron resonances are commonly used for high precision determination of masses[3,4] in more rarified clouds of trapped charges. Most of these experiments have been in the low-density "magnetron" regime, where the frequency shifts are largely determined by the applied confinement fields. However, the image charges induced on the confining conductors and the plasma shifts (similar to the upper-hybrid shift in a neutral plasma)[5] are important for a full understanding of the observed frequency shifts. The theory used to analyze such experiments was first modified to include weak space-charge effects by Jeffries *et al.*[6] Recent efforts[7] have tried to achieve better estimates of the average force between ions, including finite length effects. Image charge effects have been considered for point or line charge approximations to the ion clouds.[8–10] Gorshkov *et al.*[10] discuss the implications of having more than one species, although only for line charges orbiting at the same radius. Some of our experiments approach the magnetron regime, but most are in the plasma regime.

In our experiments, several high-frequency modes with angular dependence $\exp(il\theta)$, $l \geqslant 1$, are observed near the cyclotron frequencies of each Mg ion species. The $l=1$ modes are downshifted from the corresponding single-particle cyclotron frequencies, while the $l \geqslant 2$ modes are upshifted from the cyclotron frequencies. These shifts are related to the "diocotron" frequency, f_d, i.e., the frequency at which the plasma center-of-mass orbits around the trap axis.

The main emphasis in this work is on understanding the downshifts of the $l=1$ cyclotron modes. These downshifts are one to four times f_d, and they depend on the plasma size and composition. A multispecies, cold plasma dispersion relation quantitatively explains the observed downshifts for the majority species of Mg_{24}^{+} and Mg_{24}^{++}. This agreement includes the time evolution of the downshifts as the plasma profile evolves. The dependence of the shifts on the plasma size enables comparison of the predictions of the theory to independent measurements of the plasma profiles, thus checking the validity of the theory. Further, the dependence of the shifts on the plasma composition can be a useful diagnostic tool, enabling the nondestructive determination of the relative abundance of the various magnesium ion species in the plasma. In contrast, the $l=1$ cyclotron mode downshifts for the minority species of Mg_{25}^{+}, Mg_{26}^{+}, H_2O^{+}, and H_3O^{+} are observed to be near $-2f_d$, and do not agree with predictions of this theory.

The $l=2$ cyclotron modes of the majority species are often observed to be upshifted by $1f_d$, although families of resonances covering the range $1–2\,f_d$ are also observed. This is not predicted by the multispecies fluid theory. For the minority species, the $l=2$ resonances are only slightly upshifted; this is in qualitative agreement with the predicted upshift proportional to the species density.

The cyclotron experiments we perform not only probe the plasma, but can also change its evolution, due to heating of the resonant ions. Such heating was analyzed by Lamb, Dimonte, and Morales.[11] We find a significant improvement in the plasma confinement due to the heating. This improvement is not understood, but is probably related to more effective axial bounce averaging over field errors present in the confining volume.

[a]Present address: NCRN, P.O. 9001, Beer-Sheva 84190, Israel.

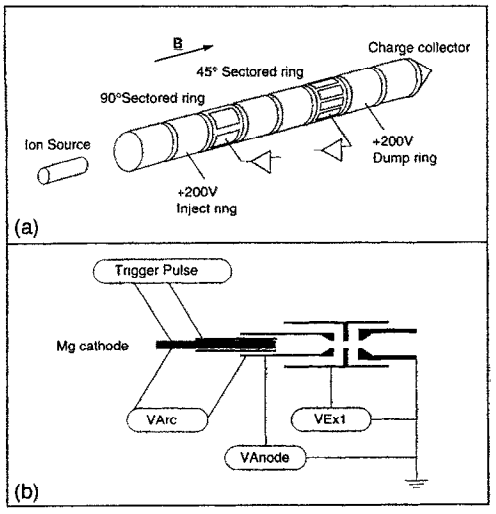

FIG. 1. (a) Schematic description of the cylindrical confinement electrodes. The sectored rings are used for excitation and detection of waves. (b) A schematic description of the Metal Vapor Vacuum Arc ion source. Typically, VArc=50 V, Trigger Pulse=8000 V, VAnode=+300 V, and VEx1=−300 V.

The manuscript is organized as follows: In Sec. II the production of the non-neutral magnesium ion plasma is described. The cyclotron resonance measurements are described in Sec. III. There the composition of the plasma, the frequency shifts of the various modes, and the determination of the exact value of the magnetic field are discussed. The theory describing the frequency shifts of the cyclotron modes is discussed in Sec. IV, and used to analyze the experimental results. In Sec. V the effect of the cyclotron heating on the plasma confinement is described. We conclude with a discussion in Sec. VI.

II. THE ION PLASMA

Schematic diagrams of the trap and ion source are given in Figs. 1(a) and 1(b). The ions are trapped in a cylindrical Penning–Malmberg trap, similar to those commonly used for pure electron plasma experiments.[1] The wall radius $R_w=2.9$ cm and the full length is $L_{\max}=45$ cm. Radial confinement is achieved with a uniform axial magnetic field B produced by a superconducting coil, with $B=15-20$ kG. The ions are axially confined by positively biased rings at the ends of the plasma column. Electron plasmas can also be produced in the same machine, using an electron-emitting spiral filament similar to that used in previous electron plasma experiments.

The magnesium ion source is a metal vapor vacuum arc (MEVVA), similar in its design to the Micro MEVVA developed at Lawrence Berkeley Laboratory.[12] The magnesium cathode is chemically but not isotopically pure, so the resulting Mg plasma has the natural abundance of the stable Mg isotopes: 79% of Mg_{24}, 10% of Mg_{25}, and 11% of Mg_{26}. Both Mg^+ and Mg^{++} are generated, and our results suggest that typically there is about three times more Mg^+ than Mg^{++} atoms. The charge fractions of each species α, denoted $\delta_\alpha \equiv Q_\alpha/Q_{\rm tot}$, are thus typically $\delta(Mg_{24}^+)\simeq 47\%$, $\delta(Mg_{24}^{++})\simeq 32\%$, $\delta(Mg_{25}^+)\simeq 6\%$, $\delta(Mg_{26}^+)\simeq 7\%$, and $\delta(Mg_{25}^{++}) \simeq \delta(Mg_{26}^{++})\simeq 4\%$.

The vacuum arc is pulsed, with a duration of about 160 μs. The ion source is located in the fringing field of the main superconducting coil, where the magnetic field is about 60 times lower than the confinement field. All the experiments reported below were performed with a fixed arc voltage of 50 V, which resulted in an arc current of about 12 A. The Mg ion beam extracted from the arc is space charge neutralized to a high degree.[13] The electrons in the beam were stopped farther downstream by applying a negative voltage (−1000 V) to a ring through which the beam flowed, leaving only unneutralized ions in the confinement region.

The voltage on the injection ring is lowered to ground about 70 μs before the arc is triggered, and is raised back to the full confining voltage of 200 V after 200 μs. When the voltage is raised, there is fast evaporation of ions for which the axial energy is high enough to overcome the potential difference between the plasma space charge potential and the confining voltages. After this initial loss, the resulting plasma has a space charge potential of about 100 V and temperature of 20–30 eV. The initial ion plasma diameter is $1.5<R_p<2$ cm, and the central density is $5\times10^7<n_0<1\times10^8$ cm^{-3}. The time when the injection gate voltage is raised will be defined as $t=0$, and all times given below are relative to this time.

The dump ring is held at +200 V throughout the injection process. Its voltage is lowered only for dumping the plasma onto a charge collector, a diagnostic technique that is inherently destructive. Nondestructive excitation and detection of waves in the plasma is performed using two sectored rings. One ring has four sectors, positioned 90° from each other and extending 58° in azimuth and 3.8 cm in length (hereafter, these sectors will be referred to as 90° sectors). The second sectored ring is built out of eight sectors, positioned at 45° from each other, each extending 27° (these sectors will be referred to as 45° sectors). Waves can be excited in the plasma by applying an oscillating voltage to one of these sectors, as will be described in the next section.

The experiments were typically performed with background pressure of $P\leqslant 2\times10^{-9}$ Torr.

III. ION CYCLOTRON RESONANCES

The measurements of cyclotron modes were performed in a single-frequency transmission mode. An oscillating voltage (typically 1.5 V) was applied to one of the 90° sectors at $z=3$ cm ($z\equiv0$ at the downstream edge of the inject ring), and the response of the plasma was detected on two of the 45° sectors at $z=37$ cm. When the frequency of the applied voltage matched a coherent oscillating mode in the plasma, the mode was excited and image charges were induced on the downstream sectors. Note that this requires the excited ions to remain coherent in their 1–2 MHz oscillations for the ~50 μs required for them to move 30 cm axially. The oscillating voltage was produced by a tracking generator, and the detected signal was processed by a spectrum analyzer locked to the frequency of the tracking generator, with a bandwidth of 300 Hz. For experiments in the "magnetron regime," where a short plasma was desired, the plasma was confined entirely within the eight-sector ring, with the signal transmitted on one 45° vector and received on another. Such experi-

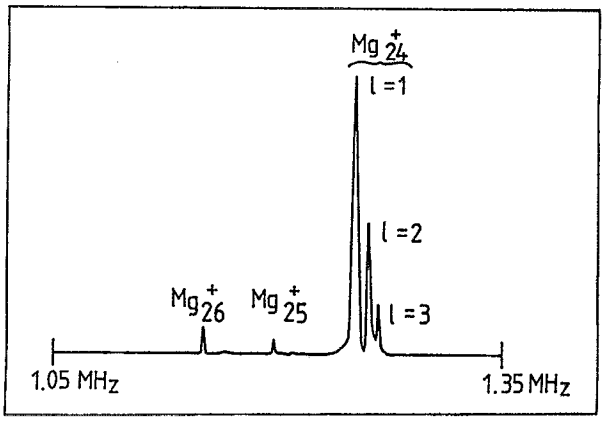

FIG. 2. Received signal versus frequency for a 300 kHz scan near the cyclotron frequencies of the Mg^+ isotopes.

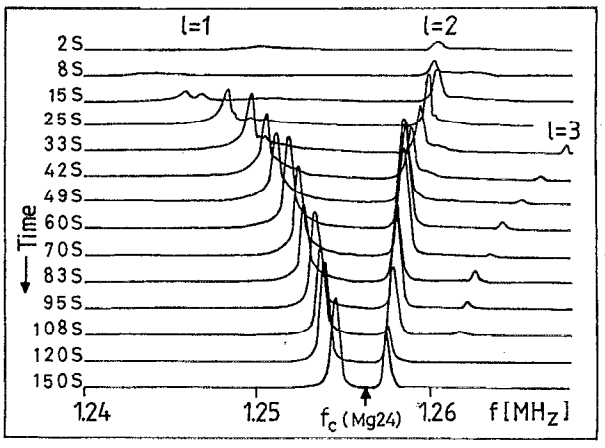

FIG. 3. Repeated frequency scans near the cyclotron frequency of Mg_{24}^+, showing the $l=1$, $l=2$, and $l=3$ azimuthal modes varying with time. All the scans were performed on a single plasma.

ments are more closely related to the work done with ion cyclotron resonance-Fourier transform mass spectroscopy (ICR-FTMS) cells.[3]

Wide frequency scans were performed in order to identify the constituent ions of the plasma. In most of the experiments, no response of the plasma was detected at frequencies other than those corresponding to the singly and doubly ionized magnesium isotopes. In one phase of the experiments, H_2O^+ and H_3O^+ ions ($M=18$ and 19 amu, respectively) were also observed. Their appearance was probably related to the addition of optical elements to the system, some covered with a hygroscopic coating. Baking the system led to the disappearance of these impurities from the ion plasmas.

In general, the ratio of the amplitudes of the resonances corresponding to the Mg^+ and Mg^{++} ions changed with time. Usually the Mg^{++} resonances decreased in time relative to the Mg^+ resonances, but in some cases the trend was inverted. We believe that this time dependence is caused by different levels of damping of the modes in the plasma, and not due to a change in the relative charge state composition of the plasma; see Secs. IV and V. It is important to emphasize that the observed amplitudes of the cyclotron modes are not proportional to the concentration of the resonant species in the plasma, and thus cannot be used to determine the relative abundance of the species in the plasma. In Sec. IV we will discuss the use of the frequency shifts of the cyclotron modes for the analysis of the plasma composition.

A. Long ion columns

Most of our experiments were performed with a long ion plasma, with $L_p \approx 45$ cm. In this case, the confining electric fields at the plasma ends contribute little to the cyclotron and diocotron mode frequencies. Data in the short plasma "magnetron regime" will be given in Sec. III B.

In Fig. 2, a frequency scan of 300 kHz shows the cyclotron modes of the three isotopes of Mg^+ at $B=20$ kG. The two lower-frequency modes are at resonant frequencies close to the cyclotron frequencies $f_c \equiv eB/mc$ of Mg_{25}^+ and Mg_{26}^+ ions. In the case of the main isotope, (Mg_{24}^+) three peaks can be observed, each slightly shifted from the exact cyclotron frequency. These modes have azimuthal mode numbers $l=1$, 2, 3.

For studying the detailed time dependence of the resonant frequencies f_{res}, repeated 30 kHz scans were performed around the relevant cyclotron frequency f_c. Each scan took about 3 s, and they were typically repeated about every 10 s, as the confined plasma slowly evolved. Figure 3 shows such repeated scans performed near the cyclotron frequency of Mg_{24}^+. The scans were obtained by applying the oscillating voltage to a single 90° sector, and detecting the transmitted signals on the second sectored ring with two adjacent 45° sectors that were connected together. Thus, modes of the form $\exp(il\theta)$ with $l=1,2$ and 3 were excited and detected. Indeed, three different modes can be observed in most of these scans. By driving different sectors with properly phased signals, the azimuthal dependence of the various modes was uniquely determined. The lower-frequency mode, downshifted relative to the cyclotron frequency, is an $l=1$ mode, while the two upshifted modes are $l=2$ (closer to the cyclotron frequency) and $l=3$.

Comparing the signals from sectors at different θ positions corroborates this identification. It was also established that the excited modes are characterized by $k_z=0$: signals taken from two sectors with the same angular position but with an axial separation of 30 cm have the same phase. This holds true irrespective of the position of the confining electrodes relative to the sector probes.

The evolution of the cyclotron resonances in Fig. 3 is due to the evolution of the plasma density and profile. Figure 4 shows measurements of the radial charge density profiles at three times, obtained from repeated dumps of similar plasmas through a movable 2.5 mm hole to a charge collector. At $t=0$ and 10 s, the plasma has a full width half-maximum (FWHM) of about 1.6 cm. Radial expansion leads to a FWHM of 3 cm at $t=60$ s, after which substantial loss of particles to the wall begins.

As can be seen in Fig. 3, the frequency shifts $f_{res}-f_c$ of all of the observed modes are decreasing with time. Such behavior was also observed in the experiments with the electron plasmas,[2] and was related to the time-dependent fre-

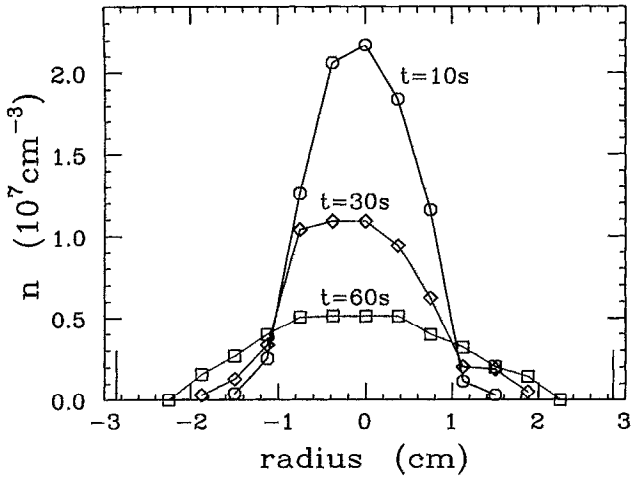

FIG. 4. Radial profiles of the ion plasma charge density $n(r,t)$ at $t=10$, 20, and 60 s.

quency f_d of the $l=1$ "diocotron" mode of the plasma. The diocotron mode is an $\mathbf{E}\times\mathbf{B}$ drift orbit of the plasma column about the axis of the confinement cylinders; it results from the asymmetric wall image charges induced when the plasma is off center. For long dense plasmas, f_d is approximately proportional to the charge per unit length, N_L, with small corrections from plasma pressure and from the end confining voltages.[14] Thus, f_d decreases as the plasma expands and loses particles. For a short plasma, this mode is more commonly called the "magnetron" mode, and the frequency is dominated by the applied confinement fields, with small corrections due to space and image charges.

We obtain the relationship between the high-frequency cyclotron modes and the low-frequency diocotron mode by measuring the time evolution of both modes in the same plasma. The diocotron mode, with $f_d \lesssim 10$ kHz, was monitored with a fast Fourier transform (FFT) frequency analyzer. In order to excite the diocotron mode, a 200 μs 5 V pulse was applied to one of the sectors; since this mode is damped within about a second, the 5 V pulses were applied every 2.5 s during the lifetime of the plasma. A typical time evolution of the diocotron frequency f_d is shown in Fig. 5. The change

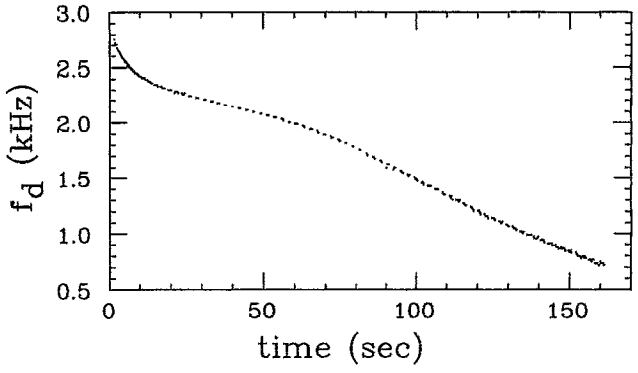

FIG. 5. Diocotron mode frequency versus time as plasma evolves.

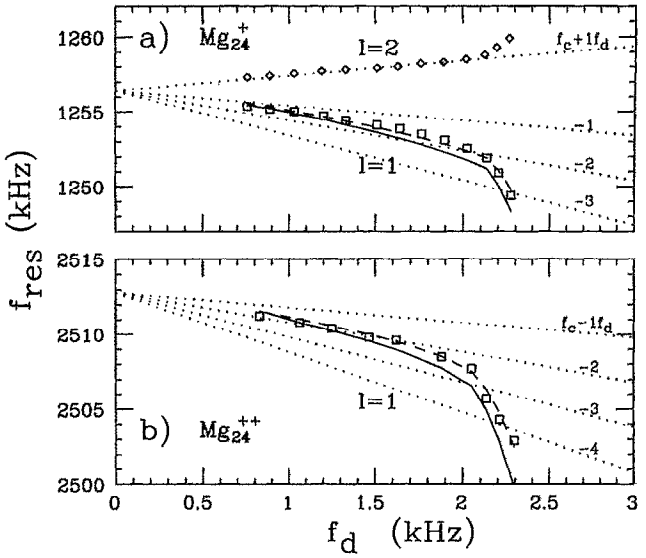

FIG. 6. (a) Frequencies f_{res} of the $l=1$ and $l=2$ cyclotron resonances near the cyclotron frequencies of Mg_{24}^{+} and Mg_{24}^{++} plotted versus the simultaneously measured diocotron frequency f_d. The solid and dashed lines are the frequencies predicted from a multispecies cold-plasma theory described in Sec. IV.

in f_d in the first 20 s is probably due to the decreasing temperature of the plasma. Afterward, the frequency is approximately proportional to the N_L.

The frequencies of the $l=1$ and $l=2$ modes near the Mg_{24}^{+} cyclotron resonances are shown in Fig. 6(a) versus the simultaneously measured diocotron frequency. The frequency of the $l=1$ mode near the Mg_{24}^{++} cyclotron resonance is similarly shown at Fig. 6(b). For both cases, the frequency of the $l=1$ mode is downshifted from the cyclotron frequencies of the plasma ions. The downshifts are about one to four times the diocotron frequency. For both Mg_{24}^{+} and Mg_{24}^{++} resonances, the ratio between the downshift and the diocotron frequency decreases with time (i.e., decreases with decreasing plasma density). The downshifts of the Mg_{24}^{++} resonances are larger than those of Mg^{+}. It should be emphasized that all the data required for either Fig. 6(a) or Fig. 6(b) were obtained from a single plasma. The time evolution of the diocotron frequency for the plasmas in Figs. 6(a) and 6(b) was almost identical.

The frequency of the $l=1$ mode was found in the electron plasma experiments[2] to be downshifted relative to the cyclotron frequency by an amount that was equal to the diocotron frequency. In Sec. IV we will relate the larger shifts observed for the $l=1$ mode in the ion plasma to the multispecies nature of this plasma. There, the ratio between the frequency shifts and the diocotron frequency will be shown to depend on the plasma size, and to decrease for an expanding plasma, in agreement with the observations. The results of the model developed there are also shown in Fig. 6 as the solid and dashed lines.

The dependence of the frequency shifts on the composition of the plasma makes the modes an important diagnostics tool. The calculated shifts shown in Fig. 6 were obtained using independent measurements of the plasma size and as-

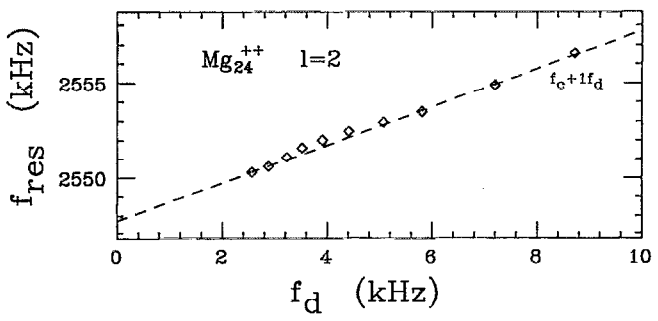

FIG. 7. Frequency f_{res} of the $l=2$ cyclotron resonance for Mg_{24}^{++} cyclotron frequency plotted versus the simultaneously measured diocotron frequency f_d.

suming a fixed ratio of 3.0 between the Mg^{+} and Mg^{++} densities, as discussed in Sec. IV. As can be seen, there is a very good agreement between the calculated shifts and the observations.

The $l=2$ resonance of Mg_{24}^{+} is seen in Fig. 6(a) to be upshifted from the cyclotron frequency, approximately by one diocotron frequency (especially for lower diocotron frequencies at later times). Similar results for the $l=2$ mode of Mg^{++} are shown in Fig. 7 for a denser plasma and slightly different magnetic field.

The single peak usually observed for the $l=2$ mode in the ion plasma is in contrast to the families of resonances observed in the electron plasma experiments.[2] However, we could also obtain such "families," as can be seen in Fig. 8, when we configured the excitation to be specific to the $l=2$ mode (connecting opposite 90° sectors together and applying signals differing by 180° to each pair). It can be seen that for most of the frequency scans, four resonance peaks were detected, with upshifts one to two times the diocotron frequency. Again, all the data shown in Fig. 8 was taken in a single experiment. The cause for the appearance of families versus a single $l=2$ modes is not presently understood.

The $l=3$ mode is seen in Fig. 3 to behave qualitatively the same as the $l=2$ mode: it is upshifted relative to the cyclotron frequency, and the shifts decrease with time (corresponding to the decrease of the diocotron frequencies). The

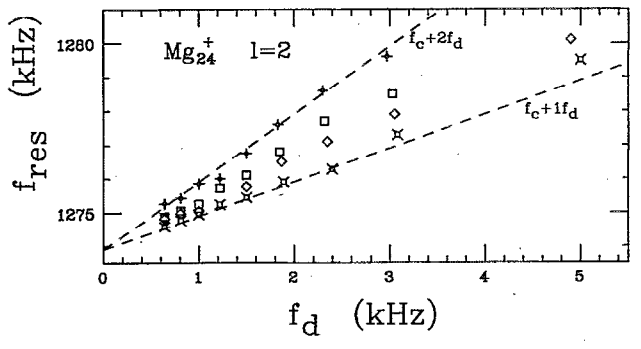

FIG. 8. Frequencies f_{res} of the family of $l=2$ cyclotron resonances near the cyclotron frequency of Mg_{24}^{+}. Such families of resonances were observed when the excitation was configured to excite only $l=2$.

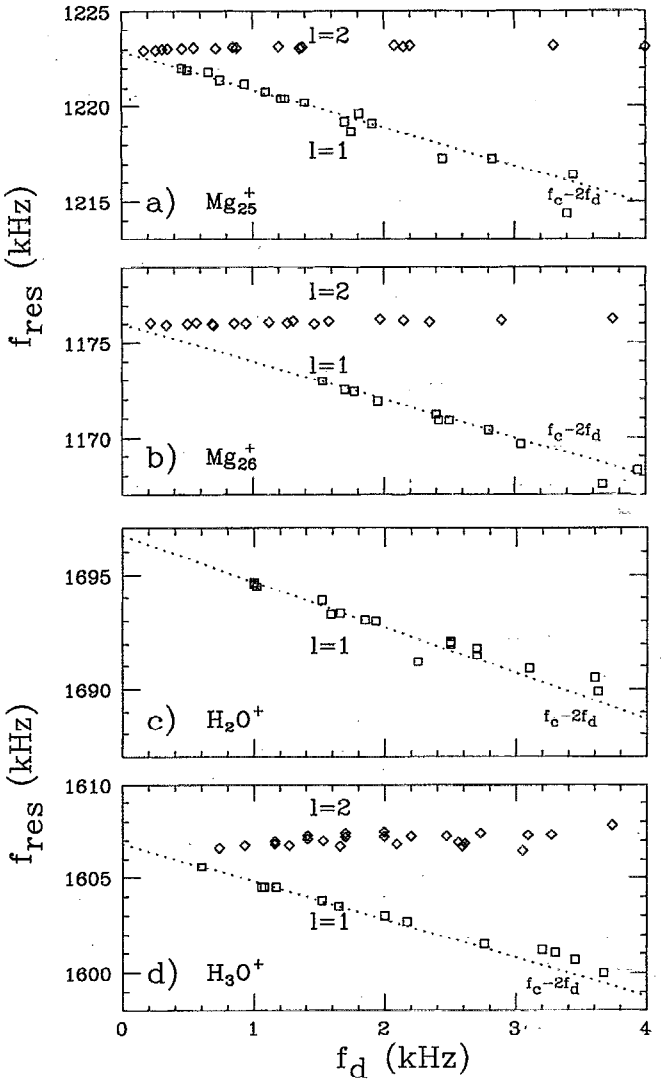

FIG. 9. The $l=1$ and $l=2$ cyclotron resonances for the minority species Mg_{25}^{+}, Mg_{26}^{+}, H_2O^{+} and H_3O^{+}. All four minority species show $f_{res}\approx f_c-2f_d$ for $l=1$, and small upshifts of the $l=2$ resonance.

shifts of the $l=3$ will not be quantitatively discussed in this report.

The frequencies of the $l=1$ and $l=2$ cyclotron resonances of the "minority" species Mg_{25}^{+} and Mg_{26}^{+} ions were also studied. For both modes the frequency shifts from the respective cyclotron frequencies were qualitatively different from those described above. The frequency of the $l=1$ mode was shifted down from the cyclotron frequency of the Mg_{25}^{+} and Mg_{26}^{+} ions by about twice the diocotron frequency, as shown in Figs. 9(a) and 9(b). This ratio between the frequency shift and the diocotron frequency was maintained over large changes in the diocotron frequency. At the experimental phase where H_2O^{+} and H_3O^{+} ions were also observed in the plasma, the frequencies of these $l=1$ modes were also found to be downshifted by twice the diocotron frequency, as seen in Figs. 9(c) and 9(d).

Subsequently, it was found that similar f_c-2f_d resonances of the $l=1$ mode can be induced, even for the "majority" Mg_{24}^{+} case by increasing the amplitude of the excita-

tion voltage. For certain conditions (the pressure higher than 10^{-8} Torr, where plasma expansion and loss are faster), the $l=1$ mode had the frequency f_c-2f_d for the entire lifetime of the plasma, even for low excitation amplitude; further, sometimes both modes at f_c-2f_d and f_c-f_d could be seen simultaneously. Although readily distinguished by the frequency versus f_d characteristics, the fundamental differences between these two modes are not understood.

The frequency shifts of the $l=2$ cyclotron mode of the minority Mg_{25}^+, Mg_{26}^+, and H_3O^+ ions were all observed to be smaller than those observed for the Mg_{24}^+ ion (Fig. 9). Qualitatively, they behaved similarly to all the other studied modes: decreasing shifts with time, and decreasing ratio between the shifts and the diocotron frequency. However, the shifts were typically only few hundred Hz, even for diocotron frequencies of several kHz. For the Mg_{25}^+ and Mg_{26}^+ resonances, the shift usually did not exceed 0.1–0.25 f_d. Larger shifts were observed for the H_3O^+ resonance, usually in the range of 0.15–0.5 f_d.

B. Magnetron regime

Qualitatively different behavior is observed for short columns in the "magnetron" regime. When the plasma is confined in just one ring (the 5.8 cm long eight-sector ring), the radial electric fields produced by the confining rings can be as large or larger than the radial field of the plasma space charge. The frequency of the diocotron mode and the frequency shifts of the cyclotron modes are then largely determined by the value of the confining voltages rather by the plasma density and composition. This situation is typical of high precision experiments with ICR cells[3] and few-particle confinement with Penning or Paul traps.[4] In that context, the diocotron mode is referred to as the magnetron mode.

Figure 10(a) shows the $l=1$ diocotron (i.e., magnetron) frequency f_d for this short ion plasma versus time for two confinement voltages. The frequency initially decays as N_L decreases, but it does not decay below a certain level determined by the confining voltage. To demonstrate the dominance of the confining electric fields, the confinement voltages were changed at $t=25-30$ s from the initial value of 40 to 200 V. The diocotron frequency changed accordingly from 1343 to 6812 Hz (a factor of 5.07).

Figure 10(b) shows the downshifts of the $l=1$ cyclotron mode of Mg_{24}^+ as a function of the diocotron frequency in the magnetron regime. For this data, a series of experiments was performed with varying confining voltages (40–250 V). In all cases, the downshifts are close to one diocotron frequency, i.e., $f_{res}=f_c-f_d$. The scatter of the results seems to be statistical in nature, limited by the accuracy of the frequency measurement, and thus study of the corrections due to space charge and image charges was not attempted. Similar downshifts, very close to one diocotron frequency, were observed for each of the plasma species.

The terms upshifts and downshifts (and the dotted lines in Figs. 6–10) assume knowledge of the exact cyclotron frequency f_c. Actually, the accuracy in determining f_c by measuring the field was less than the accuracy in extrapolating the observed resonances to $f_d=0$. The magnetic field was measured outside the vacuum chamber by a Hall-effect

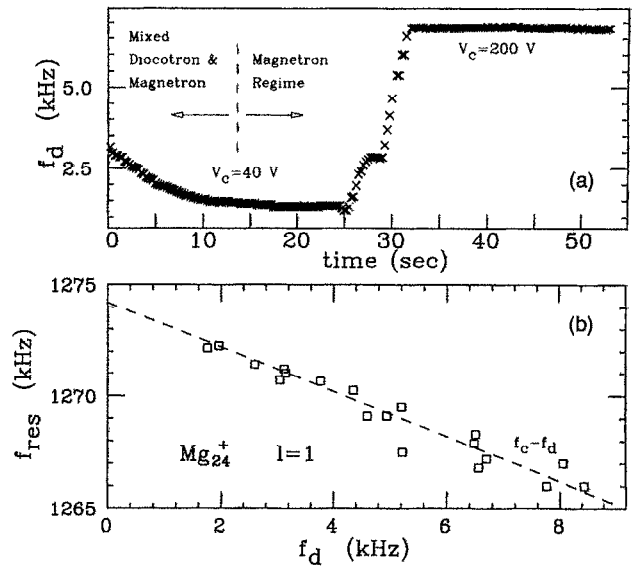

FIG. 10. (a) Diocotron (or magnetron) frequency f_d for a short plasma versus time. At time 25–30 s, the confining voltages on both end rings were raised from 40 to 200 V. (b) Frequency f_{res} of the $l=1$ cyclotron resonance of Mg_{24}^+ for a short plasma, plotted versus the diocotron frequency for confining voltages of 40–250 V.

Gaussmeter, separately calculated from the current in the superconducting magnet; both methods have an accuracy of about 10^{-3}. A better determination of the field was obtained from the cyclotron resonance measurements themselves. The downshifted $l=1$ mode and the upshifted $l=2$ mode are both converging toward an intermediate frequency, and the shifts decrease as f_d decreases.

As will be shown in Sec. IV, this limiting frequency is indeed f_c. Since the cyclotron modes were followed to shifts $\leqslant$500 Hz, it was possible to extrapolate to the zero-density limit with an estimated accuracy of about 100 Hz (or better than 10^{-4} of the main field at a field of 2 T). Comparing the values of the magnetic field obtained using frequency shifts of different ions support the estimate of 10^{-4} accuracy. It should be noted that for the above experiments, where the confined plasmas were long, the uniformity of the magnetic field over the confinement region is about equal to our accuracy in its determination, i.e., $\delta B/B \simeq 10^{-4}$.

IV. THEORY OF THE CYCLOTRON MODES

Some of the modes in non-neutral plasmas can be adequately analyzed by considering only the motion of the center of mass of the extended plasma. Indeed, the $l=1$ cyclotron and diocotron modes for single-species plasmas are essentially center-of-mass motions, as would be obtained for a single particle. In Sec. IV A, we discuss these center-of-mass motions, with the electric fields arising from the confinement fields, the plasma space charge, and the wall image charges.

However, description of the multispecies cyclotron modes requires analysis of the dispersion relation for an extended plasma, approximated as several interpenetrating cold

fluid columns. This analysis is presented and compared to the experiments in Sec. IV B, for the cases of constant and radially dependent density profiles.

A. Center-of-mass analysis

Consider the motion of a single particle moving under the combined influence of crossed electric and magnetic fields. The static electric field will be assumed to result from externally applied voltages and to depend linearly on the radius. Such a description can be used in the case of the magnetron regime, where a low-density charge cloud is confined in a short cell,[6] where the potential has the form $\Phi(r,z)=(V/2)(2z^2-r^2)$. The equations of motion in this case are

$$\ddot{x}+\Omega_c\dot{y}-Kx=0,$$
$$\ddot{y}-\Omega_c\dot{x}-Ky=0. \tag{1}$$

Here, $K\equiv 2qVG/m$ relates the externally applied voltage V to the acceleration of a particle with mass m and charge q, taking into account a factor G that depends on the geometry of the confining device. $\Omega_c=|q|B/mc$ is the cyclotron frequency of the particle.

Equation (1) has oscillatory solutions of the form $\exp(i\omega t)$, with frequencies $\omega_\pm$ given by

$$\omega_\pm=\frac{\Omega_c}{2}\left(1\pm\sqrt{1-\frac{4K}{\Omega_c^2}}\right). \tag{2}$$

For $K\ll\Omega_c^2$, the lower-frequency solution is $\omega_-\simeq K/\Omega_c$, the "magnetron" frequency, while the higher-frequency solution is approximately $\omega_+\simeq\Omega_c-K/\Omega_c$. The higher-frequency solution is downshifted from Ω_c by the magnetron frequency.

When the density of the trapped charges is small, the space charge and image charges cause only small corrections to the above expressions. Jeffries *et al.*[6] defined a space-charge modified parameter $K'=2qVG/m+4\pi q^2nG_i/m$, with G_i a geometrical factor. Such a treatment, which we shall call the "confinement fields limit," takes into account the contribution of the space charge to the electric field, but neglects the image charges.

Image charges play a crucial role in the center-of-mass motion of a plasma column confined in a long cylindrical conductor. If the plasma column shifts off center, the image charges induced on the surrounding conductor result in an orbit of the column about the trap axis at the "diocotron" frequency.

Let us now suppose that the effect of the confining fields can be neglected relative to that of the space charge and the image charges. Such a situation is typical for plasmas that are axially long relative to the diameter of the surrounding conductors. The equations of motion of the center of mass of the plasma column (neglecting all internal degrees of freedom) are actually identical in form to Eq. (1), but K is now[2] $K=\frac{1}{2}\langle\omega_p^2(r)\rangle$. Here, $\omega_p^2(r)\equiv 4\pi n(r)e^2/m$ is square of the plasma frequency due to plasma density $n(r)$, and the average $\langle\ \rangle$ is over the entire cross section of the surrounding conductor. Thus, for a plasma column with uniform density n and radius R_p, surrounded by the cylindrical conductor of radius R_w, $K=\frac{1}{2}(R_p^2/R_w^2)\omega_p^2$. For $K/\Omega_c^2\ll 1$, the lower-frequency solution is $\omega_-=\frac{1}{2}(\omega_p^2/\Omega_c)(R_p^2/R_w^2)\equiv\omega_d$, where ω_d is the diocotron frequency. As before, $\omega_-+\omega_+=\Omega_c$, and the higher-frequency solution is downshifted from the cyclotron frequency by ω_-, i.e., $\omega_+=\Omega_c-\omega_d$. We will refer to such a treatment as the "center-of-mass plasma limit." The $l=1$ cyclotron mode observed for the electron plasmas in the experiments of Gould and Lapointe[2] can be appropriately described by this limit.

Neither the "confinement fields limit" nor the "center-of-mass plasma limit" are adequate for the explanation of the frequency shifts observed in the present ion experiments. Here, the $l=1$ center-of-mass mode is downshifted from Ω_c by more than ω_d. Also, modes with $l\geqslant 2$ are not predicted by the center-of-mass analysis.

B. Multifluid analysis

To understand the large downshifts of the $l=1$ mode, the effects of the other species in the plasma must be considered. The electrostatic dispersion relation of a multispecies non-neutral plasma column has been derived by Davidson[15] for $k_z=0$, as

$$0=1-\sum_j\frac{\omega_{pj}^2[1-(R_p/R_w)^{2l}]}{2(\omega-l\omega_{rj})[(\omega-l\omega_{rj})+(-\Omega_{cj}+2\omega_{rj})]}. \tag{3}$$

This dispersion relation can be solved for any l and thus contains information on the higher l modes as well. It is derived by demanding a nontrivial perturbation solution to the linearized set of the macroscopic fluid-Poisson equations describing a cold ion plasma, i.e., the continuity, momentum, and Poisson equations. In its derivation, an idealized constant-density multispecies plasma column with radius R_p was assumed, confined inside a cylindrical conductor of radius R_w. Later in this section, we will treat the case of radially dependent density profiles.

The sum in the dispersion relation is over the species j of the plasma, and $\omega_{pj}^2\equiv 4\pi n_je_j^2/m_j$ is the square of the plasma frequency corresponding to component j. We have taken a sign convention such that Ω_{cj}, ω_{rj}, and ω are all positive.

The (slow) rotation frequency ω_{rj} of species j can be seen to be[15]

$$\omega_{rj}=\frac{\Omega_{cj}}{2}\left[1-\left(1-2\sum_i\frac{4\pi e_ie_jn_i}{m_j\Omega_{cj}^2}\right)^{1/2}\right]$$
$$\simeq\frac{\Omega_{cj}}{2}\sum_i\frac{4\pi e_ie_jn_i}{m_j\Omega_{cj}^2}$$
$$=\frac{2\pi c}{B}\sum_i e_in_i$$
$$=\sum_i\frac{\omega_{pi}^2}{2\Omega_{ci}}\equiv\omega_R. \tag{4}$$

Only the lower-frequency solutions for the rotation frequencies ω_{rj}, as appropriate to our experiment, are considered. The approximation made in expanding Eq. (4) is valid for $\omega_{rj}\ll\Omega_{cj}$, in which case mass-dependent centrifugal effects are negligible. In this approximation all the species in the plasma rotate with nearly the same rotation frequency ω_R.

For $\omega \ll \Omega_{cj}$, the dispersion relation of Eq. (3) has the solution

$$\omega - l\omega_R = -\sum_j \frac{\omega_{pj}^2}{2\Omega_{cj}}\left[1-\left(\frac{R_p}{R_w}\right)^{2l}\right], \tag{5}$$

or, using Eq. (4),

$$\omega = \omega_R[l-1+(R_p/R_w)^{2l}]. \tag{6}$$

Of special interest is the solution for $l=1$, i.e., the center-of-mass diocotron mode, which can be written as

$$\omega_d \equiv \omega_R \cdot \left(\frac{R_p}{R_w}\right)^2 = \sum_j \frac{\omega_{pj}^2}{2\Omega_{cj}}\left(\frac{R_p}{R_w}\right)^2. \tag{7}$$

In addition to these low-frequency diocotron solutions, there exist solutions of Eq. (3) near the cyclotron frequences of each of the plasma components. Let us look for the solution ω_i near the cyclotron frequency of one of the species, $\omega_i \equiv \Omega_{ci} + \Delta\omega_i$, with $|\Delta\omega_i| \ll \Omega_{ci}$. Define δ_i to be the relative charge fraction of species i in the plasma, i.e.,

$$\delta_i \equiv \frac{q_i n_i}{\Sigma_j q_j n_j}. \tag{8}$$

Assuming that $\omega_R \ll |\Omega_{ci} - \Omega_{cj}|$ for all species i, j, we can retain in the summation of Eq. (3) only the term corresponding to species i and obtain

$$\Delta\omega_i \equiv \omega_i - \Omega_{ci} = \omega_R\left\{(l-2)+\delta_i\left[1-\left(\frac{R_p}{R_w}\right)^{2l}\right]\right\}. \tag{9}$$

Equation (9) predicts, in agreement with the experimental results, that the $l=1$ resonances are downshifted, while all the $l \geq 2$ resonances are upshifted, since $\delta_i[1-(R_p/R_w)^{2l}] < 1$. This result is qualitatively the same whether the plasma is single species or multispecies. As will be seen below, Eq. (9) gives accurate quantitative predictions for the downshifts of the majority species, including the effects of plasma size and composition. However, it fails to explain the constant downshifts of the $l=1$ resonances ($\Delta f_i = -2f_d$) of the minority species.

For $l=2$ cyclotron resonances, the correspondence between theory and experiment is less satisfactory. For the majority species, the predicted upshifts are larger than f_d and decrease with increasing plasma radius, unlike the almost constant upshifts of one f_d observed in the experiments and shown in Figs. 6 and 7. For the minority species, Eq. (9) predicts small upshifts, proportional to δ_i, in qualitative agreement with the observations shown in Fig. 9.

1. Dependence on R_p

The dependence of the $l=1$ shifts predicted by Eq. (9) on the plasma radius R_p can be used to check its validity for the description of the experimental results. We will calculate R_p using the measured $l=1$ downshifts and compare it to independent measurements of the plasma radial profiles. We shall use only the Mg_{24}^+ and Mg_{24}^{++} results (the "majority" species), as only they seem to follow the predictions of Eq. (9). We shall first assume that the plasma is composed of just these two species, and then correct the analysis using our knowledge of the natural abundance of the Mg isotopes.

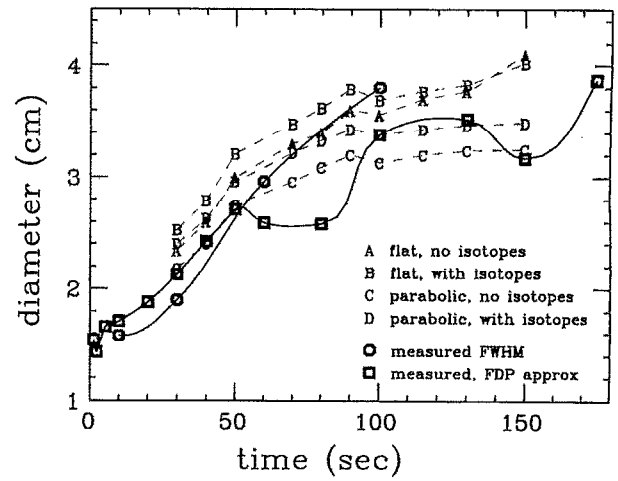

FIG. 11. Comparison of the measured and calculated plasma diameter versus time. The four dashed curves A, B, C, D show the diameters calculated from the measured $l=1$ cyclotron mode frequency shifts with four levels of approximation. Curve FWHM gives the full width half-maximum of the measured density profiles, while curve FDP shows the diameter of a flat-density-profile plasma having the same number of particles and central density as the measured plasma.

First, let us look at the $l=1$ mode in a plasma composed of just two species, α and β, representing Mg_{24}^+ and Mg_{24}^{++}, respectively. Using Eqs. (7) and (9) and $\delta_\alpha + \delta_\beta = 1$, the $l=1$ frequencies for the two species, ω_α and ω_β, can be written as

$$\begin{aligned}\Delta\omega_\alpha &\equiv \omega_\alpha - \Omega_{c\alpha} = -\omega_d - \frac{\omega_{p\beta}^2}{2\Omega_{c\beta}}\left[1-\left(\frac{R_p}{R_w}\right)^2\right],\\ \Delta\omega_\beta &\equiv \omega_\beta - \Omega_{c\beta} = -\omega_d - \frac{\omega_{p\alpha}^2}{2\Omega_{c\alpha}}\left[1-\left(\frac{R_p}{R_w}\right)^2\right].\end{aligned} \tag{10}$$

Adding these two equations and using frequencies $f \equiv \omega/2\pi$ yields

$$\frac{\Delta f_\alpha + \Delta f_\beta}{f_d} = -1 - \frac{f_R}{f_d} = -1 - \left(\frac{R_w^2}{R_p^2}\right). \tag{11}$$

Equation (11) relates the measured frequency shifts to the radius of the plasma, and can be compared to independent measurement of the plasma size. Curve A of Fig. 11 shows the plasma diameter versus time calculated from Eq. (11) and the measured frequency shifts of the $l=1$ cyclotron measurements of the Mg_{24}^+ and Mg_{24}^{++}. The measured density profiles, as in Fig. 4, are characterized by the full width half-maximum (FWHM) and by the diameter of a flat-density profile (FDP) having the measured total number of particles and central density. These measured diameters are shown in Fig. 11 by the circles and squares. Both criteria yield plasma diameters that agree with the cyclotron mode calculation to within a few mm.

The relative abundances of Mg^+ (species α) and Mg^{++} (species β) in the plasma can also be obtained from Eqs. (10):

$$\frac{\delta_\alpha}{\delta_\beta} = \frac{n_\alpha}{2n_\beta} = \frac{\Delta f_\beta/f_d + 1}{\Delta f_\alpha/f_d + 1}. \tag{12}$$

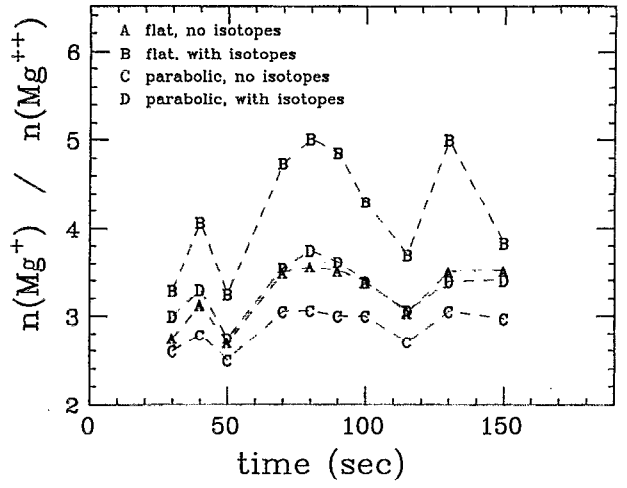

FIG. 12. Ratio between the Mg^+ and Mg^{++} number densities as a function of time calculated from the measured $l=1$ cyclotron mode frequency shifts, using the same approximations as Fig. 15.

The smaller $l=1$ downshifts of Mg^+ compared to those of Mg^{++} (Fig. 6) are thus a manifestation of the higher abundance of the Mg^+ ions in the plasma. Curve A in Fig. 12 shows the ratio between the number densities of Mg^+ and Mg^{++}, calculated using Eq. (12) as a function of time. It is calculated that there are 2.75–3.5 times more Mg^+ ions than Mg^{++} ions, and there is no clear tendency of this ratio to increase or decrease with time.

The above analysis can be easily modified to take into account the existence of the less abundant isotopes Mg_{25} and Mg_{26}, using knowledge of their natural abundances (10% and 11%, respectively). Since Mg_{24} accounts for 79% of Mg, $\delta_\alpha+\delta_\beta=0.79$, and Eq. (11) is replaced by

$$\frac{\Delta f_\alpha+\Delta f_\beta}{f_d}=-0.79-1.21 f_R/f_d$$
$$=-0.79-1.21(R_w^2/R_p^2). \tag{13}$$

The plasma diameter calculated using this expression is given in Fig. 11 by the curve marked B. It does not differ significantly from curve A. The agreement with the directly measured diameter is not improved by considering the isotopic composition within the frame of the flat-density model.

Curve B in Fig. 12 shows the ratio between the number density of the Mg^+ and Mg^{++} ions calculated when the isotopic composition is included. The difference between curves A and B in Fig. 12 is more substantial than in Fig. 11. This is to be expected, since this ratio is derived from the ratio of the shifts rather than the sum of shifts, and is more sensitive both to the underlying assumptions and to experimental errors.

2. Radial density profiles

We now examine the effects of the deviation of the plasma profile $n(r)$ from an idealized flat-density profile. We assume the same radial profile for each of the plasma species: $n_j(r) = n_{j0}*h(r)$, with $h(r=0)=1$. Experiments that looked for radial separation of the Mg^+ and Mg^{++} ions (by dumping the central portion of the plasma and looking at the cyclotron modes before and after the dumping) did not indicate any significant separation.

If we write the radially dependent rotation frequency as $\omega_R(r)=\omega_{R0}\cdot g(r)$, with $g(r=0)=1$, then $h(r)$ and $g(r)$ are related through the following differential equation:[16]

$$\frac{1}{r}\frac{d}{dr}[r^2 g(r)]=2h(r). \tag{14}$$

Again, we are looking for modes close to the cyclotron frequency of one of the plasma species. We will denote by λ_j the frequency shift from Ω_j normalized to the central rotation frequency: $\lambda_j\cdot\omega_{R0}\equiv\omega_j-\Omega_{cj}=\Delta\omega_j$. A treatment analogous to the one leading to the dispersion relation given above, investigating the possible perturbation solutions to the continuity, momentum, and Poisson equations, gives the following expression for the case of a radially dependent density profile:[17]

$$1=\frac{-2l}{R_w^{2l}}\int_0^{R_w} dr\,\frac{\delta_j h(r) r^{2l-1}}{\lambda_j-(l-1)g(r)+(1-\delta_j)h(r)}. \tag{15}$$

Equation (15), treating an arbitrary density profile $n(r)$, is the direct analog of Eq. (9) for the flat-density profile.

We now consider the case of a parabolic density profile, i.e.,

$$h(r)=\begin{cases}1-r^2/a^2, & r\leq a,\\ 0, & r>a.\end{cases} \tag{16}$$

Integrating Eq. (14) using the parabolic density profile yields $g(r)=1-\frac{1}{2}(r/a)^2$. Substituting $h(r)$ and $g(r)$ in Eq. (15) and solving for the $l=1$ mode yields

$$1=-\left(\frac{a}{R_w}\right)^2\delta_j\left[\frac{\lambda_j}{(1-\delta_j)^2}\ln\left(\frac{\lambda_j}{\lambda_j+1-\delta_j}\right)+\frac{1}{1-\delta_j}\right]. \tag{17}$$

In the limit $\delta_j\to 1$ (species j becomes the sole component of the plasma), $\lambda_j\to -a^2/2R_w^2$ and $\Delta f_j=\lambda_j\cdot f_{R0}\to -f_d$. This diocotron frequency is the same as that characterizing a flat-density plasma, with density equal to the central density of the parabolic profile and radius $R_p=a/\sqrt{2}$. Such a flat-density plasma has a diameter that is equal to the FWHM of the parabolic profile.

A numerical solution of expression (17) is given in Fig. 13 for two-species plasma with a specific parabolic profile ($a^2=R_w^2/1.5$), together with the solution for the corresponding flat-density plasma with $R_p=a/\sqrt{2}$. The shifts are given as a function of the charge fraction δ_α of one species. The solutions for the flat and parabolic profiles coincide for both $\delta_\alpha=1$ and $\delta_\alpha=0$. These two limiting cases are the single-species plasma (downshift by the diocotron frequency); and the "single-particle" limit (downshift by the rotation frequency). The shifts for a multispecies plasma ($0<\delta<1$) are an intermediate case between the two extreme limits.

In Fig. 14 the shifts near the cyclotron frequencies of Mg^+ and Mg^{++} ions are shown as a function of the FWHM diameter of a parabolic plasma ($\sqrt{2}a$), assuming a fixed composition of the plasma (three times more Mg^+ ions than Mg^{++} ions, isotopic abundances). By creating such figures for a series of abundance ratios, we determined the plasma

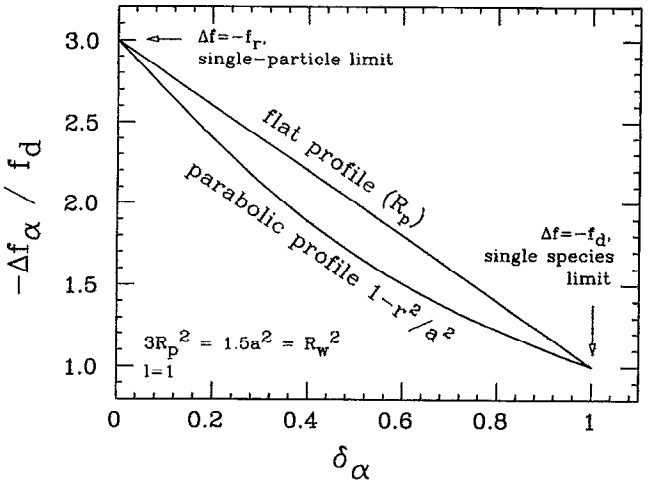

FIG. 13. Calculated frequency shifts of the $l=1$ cyclotron mode for species α, normalized to f_d, as a function of the charge fraction of species α. Calculations for both flat-density and parabolic profile plasmas are shown.

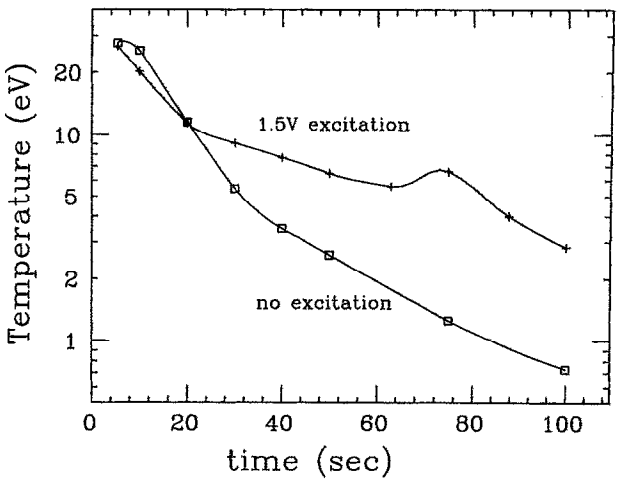

FIG. 15. Axial temperature of the ion plasma as function of time, with and without cyclotron heating.

diameter and abundance ratio that best match the measured cyclotron shifts at any given time. The resulting FWHM diameters are given in Fig. 11 as the curves marked C and D. Curve C was obtained, assuming that the $M=24$ is the only isotope, curve D by taking the actual isotopic composition into account. For both cases, the agreement to the directly measured plasma diameter (curves FWHM, FDP) is better than the flat-density calculations (curves A and B).

The ratio between the number density of the Mg^+ and the Mg^{++} ions calculated under the assumption of a parabolic profile is shown in Fig. 12, curves C and D; curve C neglects isotopic composition, while curve D includes isotopic composition. Both curves are quite similar to curve A, calculated with the flat-density model, giving $n(Mg^+)/n(Mg^{++})\approx 2.5$–$3.75$ for all times.

Alternately, we can use the independently measured plasma diameter to calculate the expected shifts near the Mg^+ and the Mg^{++} cyclotron resonances. Based on the results of Fig. 12 we assume a fixed composition, with three times more Mg^+ ions than Mg^{++} ions. A parabolic profile is assumed, and the isotopic abundance is included. The result of this calculation is shown as solid lines in Figs. 6(a) and 6(b). As can be seen, the significant features of the $l=1$ downshift is well modeled by this calculation, with no adjustable parameters. Since the plasma profile is not exactly parabolic, our definition of the plasma diameter might be biased. Adding a constant 2.5 mm to the measured plasma diameters at each time gives calculated shifts shown as dashed lines in Figs. 6(a) and 6(b); this can be thought of as a one-parameter "best fit."

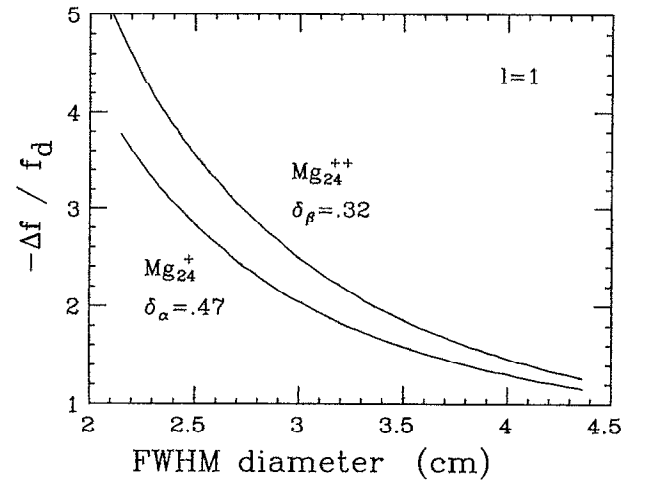

FIG. 14. Normalized frequency shifts for the $l=1$ cyclotron modes for Mg_{24}^+ and Mg_{24}^{++} ions as a function of the FWHM plasma diameter for a parabolic density profile.

V. PLASMA HEATING BY CYCLOTRON EXCITATION

Applying an oscillating voltage at a frequency close to the cyclotron frequency of one of the plasma species can lead to heating of the plasma.[9] For our plasma, this process acts in combination with two other mechanisms in determining the time dependence of the plasma temperature. (1) Electrostatic energy is converted to kinetic energy (Joule heating) as the plasma expands. This mechanism is effective mainly for early times when the density is high. (2) Collisions of the plasma ions with the background gas cool the ions. At a pressure of 10^{-9} Torr the cooling time is about 20 s, i.e., shorter than the plasma confinement time.

The axial temperature of the ions, $T_\parallel$, was measured by slowly decreasing the voltage on the dump ring and measuring high-energy ions that escape over the potential barrier, thus obtaining the tail of the velocity distribution.[18] The number of collected ions was found to increase exponentially as the voltage was decreased, justifying the use of a temperature to describe the distribution of the axial velocities. Figure 15 shows the time dependence of the measured axial temperature with and without excitation at the cyclotron frequency of Mg^+. The excitation considerably slows the ion cooling due to their collisions with the background gas.

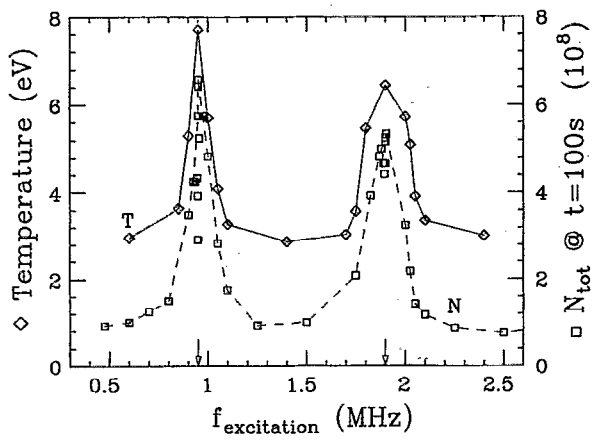

FIG. 16. Axial temperature of the plasma ions at $t=50$ s and total number remaining at $t=100$ s as a function of the excitation frequency. The excitation amplitude is 1.5 V for all frequencies. The peaks are centered around the cyclotron frequencies of Mg_{24}^{+} and Mg_{24}^{++}, i.e., 0.95 and 1.90 MHz.

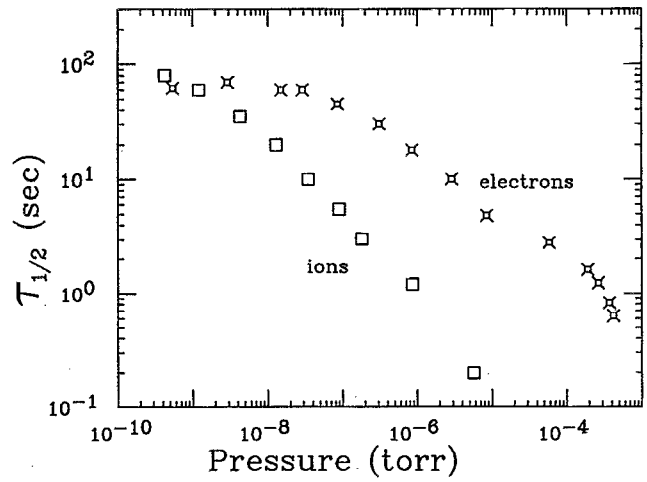

FIG. 17. Confinement times $\tau_{1/2}$ for ions and electrons at $B=20$ kG versus pressure, showing the influence of ion–neutral collisional cooling at low pressures.

Figure 16 shows the axial temperature of the ions at $t=50$ s as function of the excitation frequency. The two peaks are centered around the cyclotron frequencies of the Mg_{24}^{+} and Mg_{24}^{++} ions, i.e., 0.95 and 1.90 MHz, respectively, at $B=15$ kG.

In contrast with the resonant modes studied in previous sections, these peaks are wide, with a full width half-maximum of about 10% of the resonant frequency. This width can be attributed to the finite interaction time between the excitation and the ions. The excitation voltage is applied to a 3.8 cm long sector, for which the transit time of a 5 eV Mg ion is only 7 μs. Thus, the ions perform about ten gyrations passing through this sector ring, with the result that they can be heated even if no coherent mode is excited in the plasma.

Heating by cyclotron excitation significantly increases the plasma confinement time. This is seen both as a reduced radial expansion early in the evolution, and as a reduced loss rate to the wall late in the evolution.

Figure 16 also demonstrates the reduced loss rate of the particles to the walls by showing the number of plasma ions at $t=100$ s, N_{tot}, as function of the excitation frequency. At $t=0$ s, about 2.5×10^9 ions were captured in a plasma length of 45 cm. With no excitation, or with excitation far from the cyclotron frequencies of Mg^{+} or Mg^{++}, about 95% of the ions were lost by $t=100$ s, leaving only 1×10^8 ions in the plasma. The number remaining increased more than six-fold when the plasma was excited near the cyclotron frequency of either of the Mg^{+} or Mg^{++}. The N_{tot} peaks in Fig. 16 have a similar width to the temperature peaks, with FWHM being about 10% of the resonant frequency. Excitation at the third and fourth harmonic of the Mg_{24}^{+} resonance did not lead to heating or improvement of the confinement of the plasma.

This temperature dependence of the ion confinement results in a pressure-dependent loss rate, since ion–neutral collisions cool the ions. A pressure dependence of the confinement time is also observed for electrons,[19] but is significant only for $P>10^{-7}$ Torr when the collision-induced transport is comparable to the transport due to field errors. Figure 17 shows the dependence of $\tau_{1/2}$ (the time when half of the initial number of charges are lost) on the pressure for both electrons and ions (obtained in the same machine and the same magnetic field). The electron confinement time is indeed independent of pressure for $P<10^{-7}$ Torr, as was observed in previous experiments. On the other hand, the ion confinement still improves as the pressure is lowered, even for $P\leq10^{-9}$ Torr.

Similar (although not identical) temperature evolutions can be obtained at two different values of background pressure if cyclotron heating is applied in the higher-pressure case to compensate for the greater collisional cooling. Such comparisons showed that indeed the pressure dependence of the confinement times of the ions for $P\simeq10^{-9}$ Torr is only due to the changing cooling rate. In Fig. 18, we plot the plasma loss time τ_L versus temperature for $P=7\times10^{-10}$

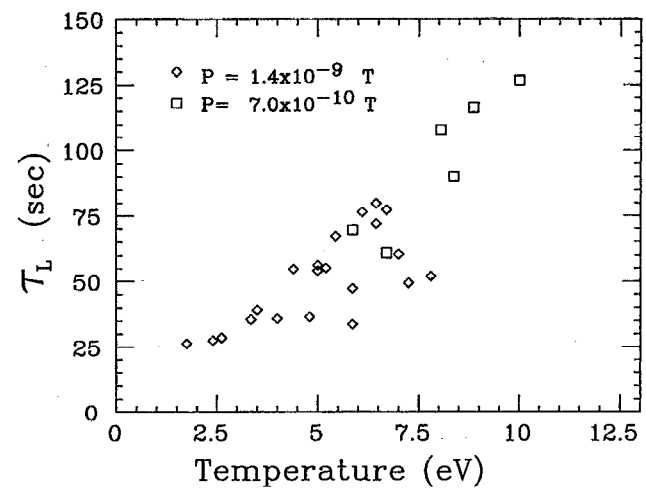

FIG. 18. Characteristic time τ_L for decrease of the plasma line density from $t=60-80$ s versus the axial temperature measured at $t=80$ s. The measurements were performed at $P=7\times10^{-10}$ and 1.4×10^{-9} Torr with varying levels of cyclotron heating.

and $P=1.4\times10^{-9}$ Torr. At each pressure the temperature was adjusted by adjusting the excitation frequency. The loss time τ_L (obtained in a way described below) appears to be affected by background pressure mainly through the resulting change in ion temperature.

The data shown in Fig. 18 were taken with the aim of quantifying the dependence of the plasma loss rate on its axial temperature. Since the temperature measurement is destructive, it was important to measure the loss rate of the plasma just before dumping it, over a period when the temperature was not varying rapidly. This was accomplished by measuring the rate of decrease of the diocotron frequency (proportional to the plasma line density) at $t=60-80$ s and measuring the temperature at $t=80$ s. For $t=60-80$ s the diocotron frequency was decreasing nearly exponentially, since the plasma was then losing particles to the wall with a rate $(\ln 2)\tau_L^{-1}=(df_d/dt)/f_d$. Thus, τ_L is the time over which the density would decrease by half. It can be seen that the loss time is approximately linear with the axial temperature. To date, we have no explanation for this effect.

VI. DISCUSSION

The shifts of the $l=1$, $l=2$, and $l=3$ modes from the Mg ion cyclotron frequencies are qualitatively similar to shifts observed for electrons: the $l=1$ mode frequency is shifted downward, while the frequency of the $l=2$ and $l=3$ modes is higher than the cyclotron frequency. However, significant quantitative differences exist between the ion results and the electron results, because of the multiple species in the ion plasma.

For the electron plasma, the $l=1$ mode was found to be downshifted from the cyclotron frequency by an amount equal to the diocotron frequency. In the ion plasma, the shifts are larger than the diocotron frequency (up to four f_d in the case of the Mg_{24}^{++} ions), and are different from species to species. The derivations of Sec. IV show that these frequency shifts can be understood when the existence of several species in the plasma is taken into account. Good agreement was obtained between the diameter of the plasma calculated from cold fluid theory applied to the measured cyclotron frequency shifts, and the directly measured plasma diameter, as shown in Fig. 11. Four different levels of approximation were compared (flat versus parabolic density profiles, each with or without taking into account the existence of several isotopes). It was found that the differences between the results of these four approximations are relatively small. As can be seen in Fig. 6, the measured shifts near the cyclotron frequencies of both Mg_{24}^{++} and Mg_{24}^{++} can be explained by the theory with a fixed ratio between the abundance of these ions. The time dependence of these shifts is readily explained by the time evolution of the plasma profile.

As was seen in Sec. IV, the theory for the multispecies plasma ranges between two limiting cases. On the one extreme, there is the single-species plasma ("center-of-mass plasma limit"). Its $l=1$ frequency downshift equals one diocotron frequency, and can be understood by the interaction between the center of mass and the induced image charge, neglecting all internal degrees of freedom. The single-species electron plasma is adequately described by this picture. On the other extreme is the "single-particle" limit for a very dilute minority species. In this case most of the shift is caused by electric fields that are generated by the other species, and the predicted downshift is the rotation frequency of the plasma. This limit resembles the "confinement-fields" limit discussed in Sec. IV, where for a short plasma the radial electric fields are generated mainly by the confinement fields and not by the excited particles.

Our results in the magnetron regime (confinement of a short plasma) matched the prediction of downshifts of one f_d. On the other hand, we did not observe the predicted single-particle behavior in the case of the long plasma, even for the cyclotron modes of the minority Mg_{25}^{+} and Mg_{26}^{+} ions. Instead, a downshift of two f_d was measured. The observation of a similar behavior for the Mg_{24}^{+} ions when the excitation amplitude was high enough seems to suggest that some nonlinear process may change the nature of the mode. Further investigation is required for understanding this regime.

Our results strongly suggest that the amplitude of the detected mode cannot be used as a reliable measure for determining the relative abundance of the plasma species. This is probably due to mode damping, which depends on the species abundance. On the other hand, the frequency shifts of the $l=1$ cyclotron mode of the majority species also turn out to be dependent on the relative concentration of this species in the plasma, and thus can be used as an important diagnostics tool.

The upshifted $l=2$ cyclotron mode is less well understood than the $l=1$ mode. Usually we observed upshifts of about one diocotron frequency for the $l=2$ resonances of Mg_{24}^{+} and Mg_{24}^{++}. However, when the drive was tailored for the excitation of only the $l=2$ mode, a family of up to four peaks was obtained between f_c+f_d and f_c+2f_d. Such families of resonances were explained for the electron plasma[2] by considering the effects of the finite temperature of the plasma, and adapting the theory of trapped Bernstein modes to the case of the non-neutral plasma. This analysis does indeed yield families of resonances, with spacings of $2(R_c/R_p)\ \omega_{R0}$, where R_c is the ion Larmor radius. This analysis predicts that as the plasma expands (R_p increases) and the ions cool (R_c decreases) the spacing between the resonances (normalized to f_d) should decrease. This prediction is in contradiction to the observed data of Fig. 8, where the spacings were nearly constant multiples of f_d.

The cold-plasma theory developed in Sec. IV predicts $l=2$ upshifts that are proportional to the relative abundance of the resonant species [Eq. (18)]. For majority species this yields excessively large upshifts compared with the observed upshift of $1-2\ f_d$. For minority species like Mg_{25}^{+} and Mg_{26}^{+} with charge fraction $\delta\simeq6\%-7\%$ small frequency shifts are to be expected, as was indeed observed. The size of these frequency shifts, $0.1-0.25\ f_d$, yield reasonable estimates for the relative abundance of these isotopes, when Eq. (18) is used, together with an independent measurement of the plasma size. However, since only small shifts are involved, it was difficult to determine the level to which the cold-plasma theory successfully describes these observations.

The heating of the ions due to an oscillating voltage close to their cyclotron frequency was investigated by Lamb,

Dimonte, and Morales.[11] There, a single pass of ions through a localized excitation region was considered. The heating was analyzed in terms of the breaking of the adiabatic condition $|\omega-\Omega|L/v_z \gg 1$, where L is the length of the excitation region and v_z is the ion axial velocity. The range of frequencies over which this condition is violated roughly matches the range of frequencies where heating of the plasma was observed in our experiments. It should be noted that our temperature measurement probed only the axial velocity distribution, while the theory[9] predicts mainly a change in the perpendicular energies. However, the collision time is short enough for transfer of perpendicular to parallel energy to occur. Future laser-induced fluorescence can further probe the velocity distribution in both directions, and quantify the efficiency of the temperature equilibration.

We believe that it is indeed the increased axial velocities that are responsible for the improved confinement observed for the cyclotron-heated plasmas (and equivalently, for the better confinement at lower pressures). The nature of the responsible mechanism is not well understood, but it is probably related to the faster bouncing motion of the ions, leading to better bounce averaging over the magnetic field errors that inevitably exist. Resonant-particle transport theories[20] emphasize the importance of the ratio between the bounce to rotation frequencies. However, it is found in our experiments that the heated and better-confined plasmas do not necessarily have a higher ratio of the bounce to the rotation frequency. This is due to the higher rotation frequency characterizing the better-confined plasmas. Thus, both theoretical and experimental effort are required in order to achieve better understanding of this phenomenon.

ACKNOWLEDGMENTS

We wish to thank R. W. Gould and T. M. O'Neil for their contribution to the theoretical understanding of the observed shifts. We thank I. G. Brown for his help in designing the ion source. The technical help of R. Bongard is appreciated.

The research is supported by Contract No. ONR N00014-89-J-1714.

[1] See, for example, *Non-Neutral Plasma Physics*, AIP Conf. Proc. 175, edited by C. W. Roberson and C. F. Driscoll (American Institute of Physics, New York, 1988).
[2] R. W. Gould and M. A. LaPointe, Phys. Fluids B **4**, 2038 (1992).
[3] *Fourier Transform Mass Spectrometry*, American Chemical Society Symposium Series 359, edited by M. V. Buchanan (American Chemical Society, Washington, DC, 1987).
[4] G. Gabrielse, X. Fei, L. A. Orozco, R. L. Tjoelker, J. Haas, H. Kalinowsky, T. A. Trainor, and W. Kells, Phys. Rev. Lett. **65**, 1317 (1990).
[5] S. A. Prasad, G. J. Morales, and B. D. Fried, Phys. Fluids **30**, 3093 (1987).
[6] J. B. Jeffries, S. E. Barlow, and G. H. Dunn, Int. J. Mass Spectrom. Ion Proc. **54**, 169 (1983).
[7] S. P. Chen and M. B. Comisarow, Rapid Commun. Mass Spectrom. **5**, 450 (1991); **6**, 1 (1992).
[8] R. S. Van Dyck, Jr., F. L. Moore, D. L. Farnham, and P. B. Schwinberg, Phys. Rev. A **40**, 6308 (1989).
[9] X. Xiang, P. B. Grosshans, and A. G. Marshall, Int. J. Mass Spectrom. Ion Proc. **125**, 33 (1993).
[10] M. V. Gorshkov, A. G. Marshall, and E. N. Nikolaev, J. Am. Soc. Mass Spectrom. **4**, 855 (1993).
[11] B. M. Lamb, G. Dimonte, and G. J. Morales, Phys. Fluids **27**, 1401 (1984).
[12] I. G. Brown, J. E. Galvin, R. A. MacGill, and R. T. Wright, Appl. Phys. Lett. **49**, 1019 (1986).
[13] H. Shiraishi and I. G. Brown, Rev. Sci. Instrum. **61**, 3775 (1990).
[14] K. S. Fine, Phys. Fluids B **4**, 3981 (1992).
[15] R. C. Davidson, *Physics of Nonneutral Plasmas* (Addison–Wesley, Redwood City, CA, 1990), p. 258.
[16] R. H. Levy, Phys. Fluids **11**, 920 (1968).
[17] R. W. Gould, Phys. Plasma **2**, 1404 (1995).
[18] B. R. Beck, J. Fajans, and J. H. Malmberg, Phys. Rev. Lett. **68**, 317 (1992).
[19] J. H. Malmberg and C. F. Driscoll, Phys. Rev. Lett. **44**, 654 (1980).
[20] D. L. Eggleston, T. M. O'Neil, and J. H. Malmberg, Phys. Rev. Lett. **53**, 982 (1984).